Available online at www.sciencedirect.com

ScienceDirect

Ceramics International 40 (2014) 1901–1908

CERAMICS INTERNATIONAL

www.elsevier.com/locate/ceramint

Monoclinic Li_2TiO_3 nano-particles via hydrothermal reaction: Processing and structure

Cheng-Long Yu[a,b], Kazumichi Yanagisawa[b,*], Sumio Kamiya[c], Takahiro Kozawa[d], Tadaharu Ueda[e]

[a]School of Materials Science and Engineering, Shaanxi University of Science & Technology, Xi'an 710021, PR China
[b]Research Laboratory of Hydrothermal Chemistry, Faculty of Science, Kochi University, Kochi 780-8520, Japan
[c]Toyota Motor Corporation, 1, Toyota-cho, Toyota, Aichi 471-8572, Japan
[d]Joining and Welding of Research Institute, Osaka University, Osaka 567-0047, Japan
[e]Department of Applied Chemistry, Faculty of Science, Kochi University, Kochi 780-8520, Japan

Received 6 June 2013; received in revised form 16 July 2013; accepted 18 July 2013
Available online 26 July 2013

Abstract

Pure phase Li_2TiO_3 nano-particles were synthesized via hydrothermal reaction using anatase TiO_2 and $LiOH \cdot H_2O$ at 200 °C. No development of the (002) supercell diffraction peak is exhibited in the XRD pattern. In contrast, by further calcination above 500 °C for 6 h in air, full development of the (002) supercell diffraction peak is observed. TEM observation and particle size analysis indicate that the general particle size is around 114 nm. HR-TEM observation and the 2D FFT analysis show that the layered structure corresponding to the LiTi2 layer is clearly developed. During calcination, additional Li ions diffuse into the supercell, corresponding with the diffusion of Ti ions away from the interslab into the slab, forming a more stable structure. Lithium insertion, corresponding with dissolution and precipitation mechanism is proposed for the formation of Li_2TiO_3.

Keywords: Monoclinic Li_2TiO_3 fine particles; Hydrothermal reaction; Anatase TiO_2; Structure; Formation mechanism

1. Introduction

In a fusion reactor, the breeder materials play essential role in producing tritium atoms by lithium transmutation, $^6Li+n \rightarrow {}^4He+T$, where n is neutron and T is tritium. Lithium based ceramics have been considered as ideal candidate for tritium breeding in both the helium cooled pebblebed blanket for DEMO and the ITER testing blanket due to their high thermal conductivity, as well as satisfactory breeding performances [1]. Monoclinic Li_2TiO_3 is regarded as one of the most appropriate candidates for the solid tritium breeder materials in D–T fusion reactors owing to its fairly good tritium release property at low temperatures between 200 °C and 400 °C and its lower activation performances [2–4].

There have been many published reports on the preparation methods of Li_2TiO_3 particles. Conventionally, Li_2TiO_3 is produced by solid state reaction of mixture of Li_2CO_3 and TiO_2 at 900–1100 °C for 10 h to several days [5–7]. In 2009, Kataoka and co-workers prepared single crystal Li_2TiO_3 for determination of the structure by solid state reaction [8]. Other typical wet chemical methods include the sol–gel method [9], the combustion synthesis method [10,11], and the polymer solution method [12].

To our knowledge, up to date, few reports on the synthesis of Li_2TiO_3 using microsized TiO_2 powder as raw materials via hydrothermal reaction have been published [13]. In this article, the Li_2TiO_3 nano-particles were synthesized via hydrothermal reaction using anatase TiO_2 and $LiOH \cdot H_2O$ at 200 °C for 10 h. No complicated process was needed compared with the sol–gel method, and the combustion synthesis method, although the hydrothermal reaction conditions will determine the final phase. According to our previously published articles on correlated titanates [14], the structure and formation mechanism of Li_2TiO_3 was discussed as well.

*Correspondence to: Research Laboratory of Hydrothermal Chemistry, Faculty of Science, Kochi University, 2-5-1, Akebono-cho, Kochi-shi, 780-8520, Japan. Tel.: +81 88 844 8352; fax: +81 88 844 8362.
E-mail addresses: yanagi@kochi-u.ac.jp, yanagi@cc.kochi-u.ac.jp (K. Yanagisawa).

0272-8842/$ - see front matter © 2013 Elsevier Ltd and Techna Group S.r.l. All rights reserved.
http://dx.doi.org/10.1016/j.ceramint.2013.07.097

2. Experimental procedure

2.1. Preparation

The typical experimental process is given hereby. 1.198 g (0.015 mol) TiO_2 powders (Anatase phase, Wako Pure Chemical Industries, Ltd., Japan) and 1.259 g (0.03 mol) $LiOH \cdot H_2O$ (Wako Pure Chemical Industries, Ltd., Japan) powders were added into the Teflon lined autoclave (~25 mL) together with 15 mL distilled water. The mol ratio of $LiOH \cdot H_2O$ to TiO_2 was fixed to be 2:1 and the LiOH concentration was 2 mol/L. In order to investigate the formation mechanism of Li_2TiO_3, the above mixture was heated at 50 °C, 100 °C, 150 °C, 175 °C for 1 h. Additionally, the mixture was held at 200 °C for varied lengths of time from 2 h to 10 h. The as-prepared particles were dried at 50 °C in ambient conditions. Then the dried particles were calcined at 500 °C and 600 °C for 6 h in ambient conditions.

In order to understand the effect of distilled water on the structure evolution of TiO_2, the TiO_2 powders were treated in pure distilled water at 200 °C for 10 h. The as-prepared powders were dried at 50 °C in ambient conditions for further characterization.

2.2. Characterization

The phase identification of the dried particles was conducted by the X-ray diffraction analysis. The diffraction patterns were collected with a Rigaku Ultima IV diffractometer with CuK_α radiation ($\lambda = 1.540$ Å). The patterns of the raw TiO_2 powders and that hydrothermally treated in distilled water were refined using the profile fitting tool in the software Jade (Version 5.0). The crystallite size of both TiO_2 and Li_2TiO_3 is calculated based on the FWHM (full width at half maximum) corresponding to lattice plane (101) of TiO_2 and lattice plane (−133) of Li_2TiO_3 by the Scherrer equation $d = K\lambda/\beta \cos\theta$, where K is a constant identified as 0.85; λ is the wavelength of the X-ray; β is the FWHM; and θ is half the $2\theta^\circ$ in the XRD pattern.

The morphology of the fine particles was observed by transmission electron microscopy (TEM, H-800, Hitachi Ltd., Tokyo, Japan) operated at 200 kV and field emission scanning electron microscopy (FE-SEM, JSM-7600F, JOEL Ltd. Japan). HR-TEM and SAED of the dried and annealed powders were conducted by the transmission electron microscopy (HR-TEM, H-9500, Hitachi Ltd., Tokyo, Japan) operated at 300 kV.

The particle size analysis was conducted in an ultraviolet laser nano-particle size analyzer (SALD-7100, Shimadzu Corporation, Japan) with ultrasonic dispersion in distilled water for 1 h before analysis.

The chemical composition of the powder was determined by inductively coupled plasma atomic emission spectroscopy (ICPE-9000, Shimadzu Corporation, Japan). Before measuring, the powder was dissolved in aqua regia.

3. Results and discussion

3.1. Characterization of the raw TiO_2 particles

XRD patterns of the raw anatase TiO_2 particles and that by hydrothermal treatment in distilled water at 200 °C for 10 h are given in Fig. 1(a) and (b), respectively. According to Fig. 1(a), the raw particles are of well crystallized anatase phase (JCPDS card no. 21-1272) and the cell type is tetragonal with the space group I41/amd (No. 141), $Z = 4$. No phase transformation takes place during hydrothermal treatment in water. However, the corresponding peak intensity decreases drastically after hydrothermal treatment. The parameters and values via refinement before and after hydrothermal treatment are listed in Table 1.

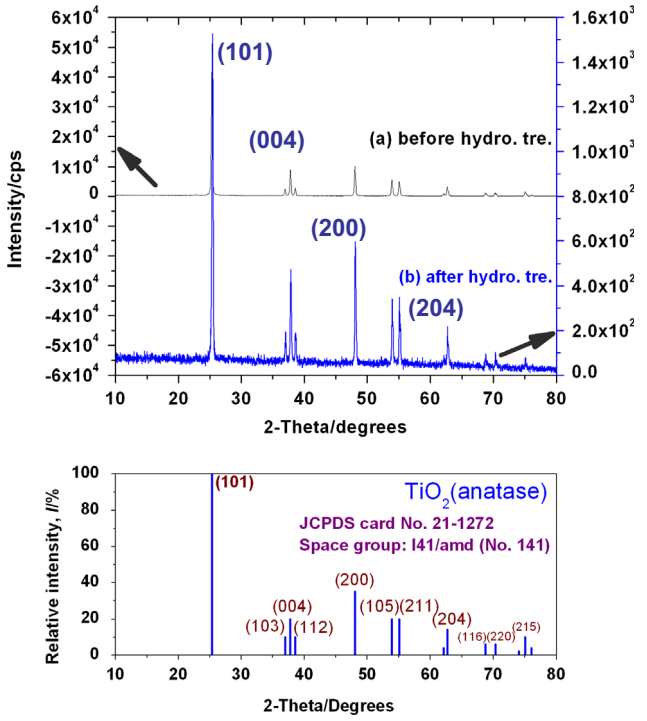

Fig. 1. XRD patterns of the TiO_2 particles, (a) before hydrothermal treatment and (b) after hydrothermal treatment.

Table 1
Refinement results for the XRD patterns.

Structural formula	TiO_2 (before hydro. tre.)	TiO_2 (after hydro. tre.)
Temperature	295 K	295 K
Cell type	Tetragonal(I-center)	Tetragonal(I-center)
Space group	I41/amd (No. 141)	I41/amd (No. 141)
Lattice parameters		
***a, b* (Å)**	3.78549(0.000125)	3.77874(0.001395)
***c* (Å)**	9.51386(0.000534)	9.50113(0.006334)
***V* (Å^3)**	136.33	135.67
Z	4	4
Density (g/cm^3)	3.8927	3.9118
Maximum 2-theta	80°	80°
Crystallite size	53.8(0.8)nm	36.9(2.0)nm
R_p	9.88%	19.75%

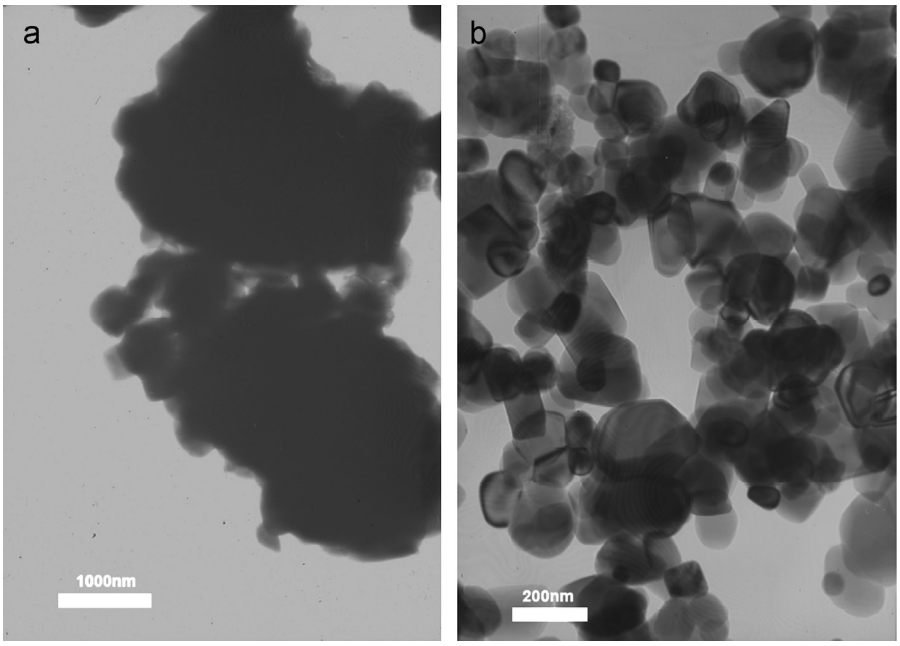

Fig. 2. TEM images of (a) the raw anatase TiO_2 particles and (b) that after hydrothermal treatment at 200 °C for 10 h.

The crystallite size before and after hydrothermal treatment is 53.8 nm and 36.9 nm, respectively, indicating the crystallite size of TiO_2 drastically decreases by hydrothermal treatment. Additionally, the R_p value increases from 9.88% to 19.75%, serving as an evidence of the decrease of crystallization perfection. TEM images of the anatase TiO_2 particles and that after hydrothermal treatment at 200 °C for 10 h are given in Fig. 2(a) and (b), respectively. It is obvious that the particle size decreases after hydrothermal treatment. Before hydrothermal treatment, the particle size is about several microns, while after hydrothermal treatment that is ranging from 50 nm to 200 nm, possibly resulting from the dissolving of the TiO_2 during hydrothermal treatment. It can be estimated that during hydrothermal reaction in LiOH solution, TiO_2 will be dissolved more, resulting from the alkaline conditions.

3.2. Phase evolution, morphology observation and particle size analysis

XRD patterns of the Li_2TiO_3 particles via hydrothermal reaction and that calcined at 500 °C and 600 °C for 6 h are given in Fig. 3. Development of (−133) diffraction peak is exhibited in XRD pattern of the as-hydrothermally prepared particles, suggesting the well ordering of lithium ions and titanium ions in the slab (the LiTi2 layer), as the formula of a well ordered Li_2TiO_3 can be written as $Li_{interslab}(Li_{1/3}Ti_{2/3})_{slab}O_2$, where in the slab lithium ions occupy 1/3 the 4e sites while the titanium ions occupy 2/3 the other 4e sites [8]. No development of supercell diffraction peak (002) is exhibited via hydrothermal reaction, indicating the disordering of the lithium ions in the interslab. It needs to be addressed that the amorphous like diffraction pattern around 20° 2-theta degrees is ascribed to the diffraction of residual $LiOH \cdot xH_2O$ $(0 < x < 1)$.

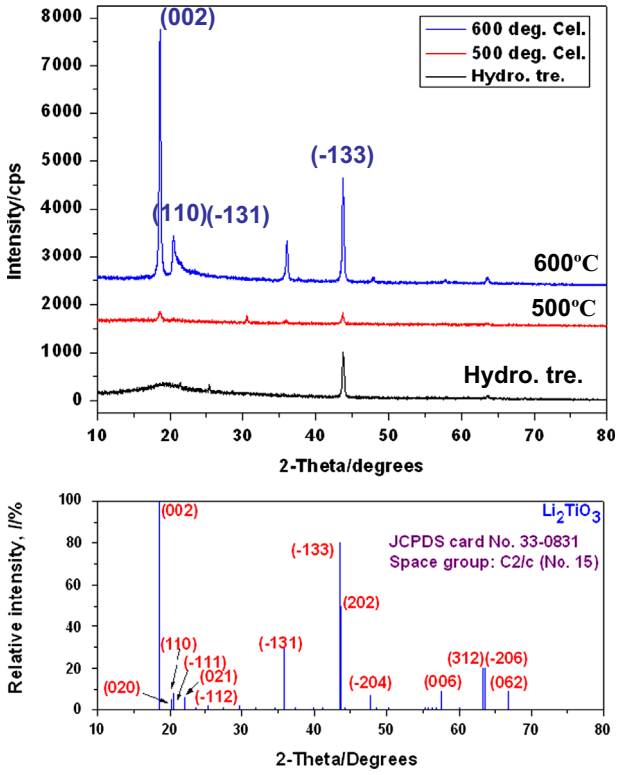

Fig. 3. XRD patterns of the particles via hydrothermal reaction and that calcined at 500 °C and 600 °C for 6 h respectively.

Development of the supercell diffraction peak (002) is exhibited for the particles calcined at 500 °C for 6 h, indicating that additional activation energy is required for ordering of lithium ions in the interslab. A higher calcination temperature at 600 °C for 6 h is beneficial to the increase of the (002) peak intensity and the development of (110) diffraction peak (Fig. 3).

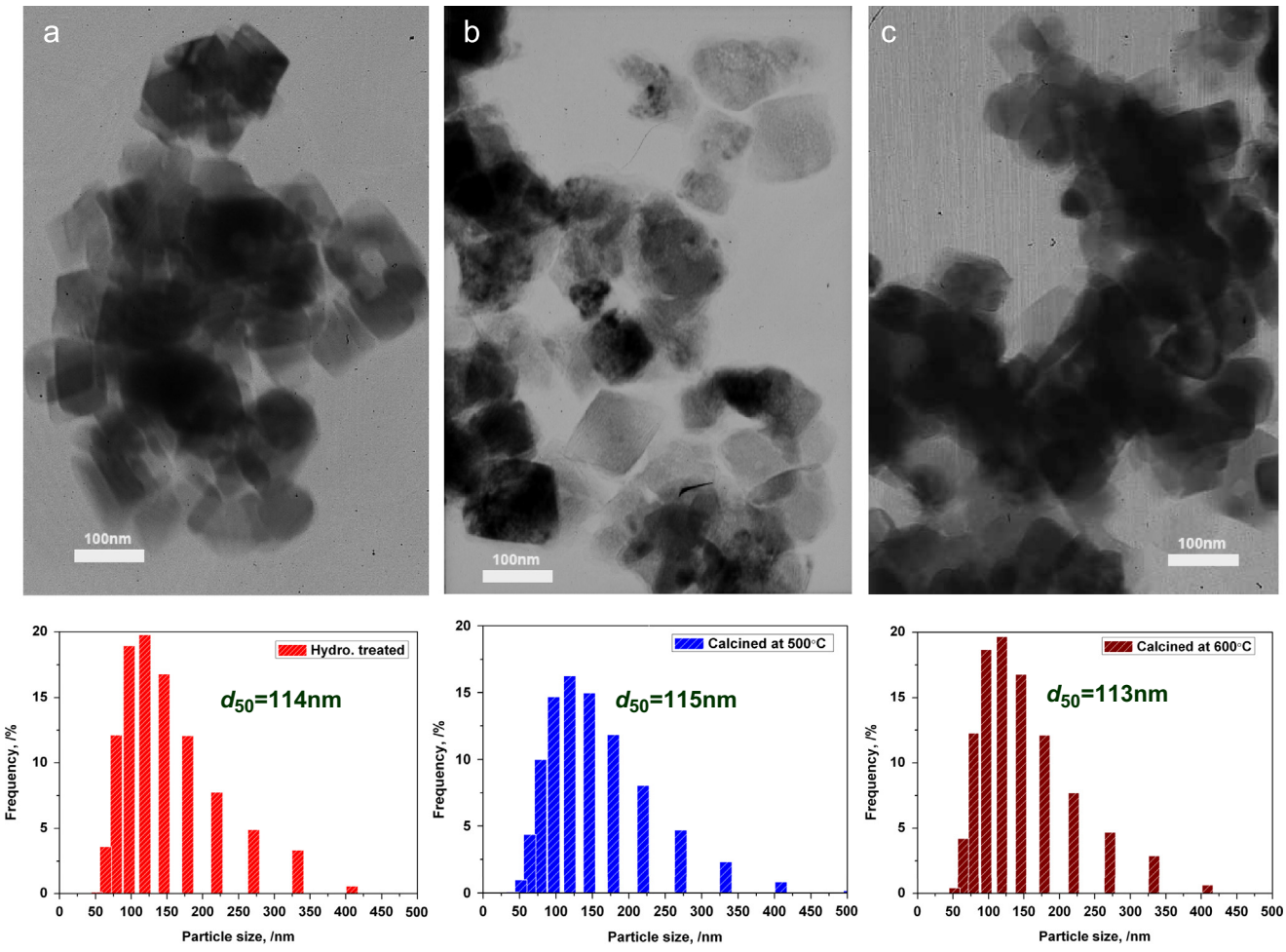

Fig. 4. TEM image and the particle size analysis result of the particles via hydrothermal reaction (a), and calcined at 500 °C (b), 600 °C (c) for 6 h.

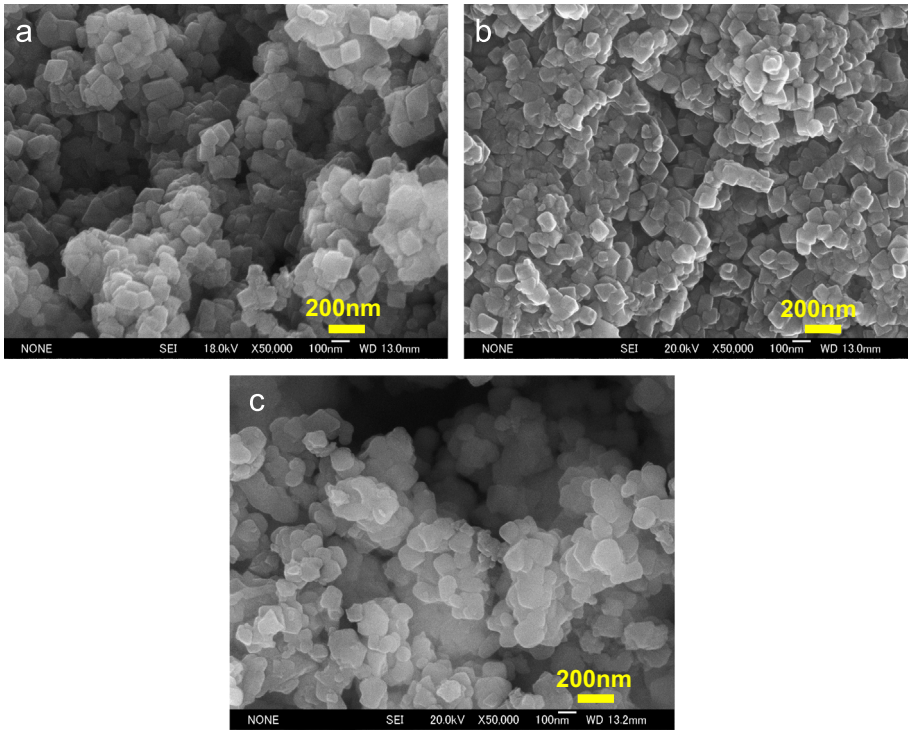

Fig. 5. FE-SEM micrographs of the Li_2TiO_3 particles, (a) via hydrothermal reaction; (b) via further calcinations at 500 °C; and (c) via further calcinations at 600 °C.

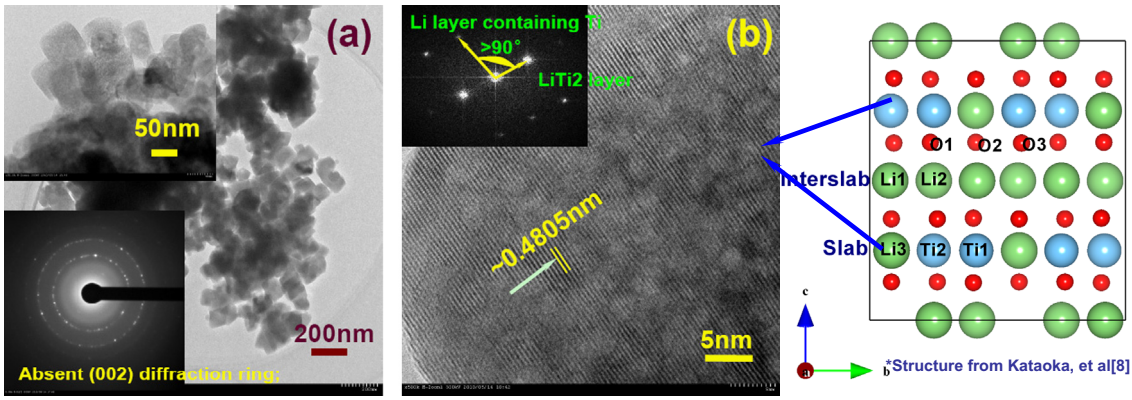

Fig. 6. (a) TEM image and SAED pattern (the inserted lower-left) and (b) HR-TEM image and 2DFFT pattern (the inserted upper-left) of the Li_2TiO_3 by hydrothermal reaction. The inserted graph in the right of (b) gives the illustration of a perfect supercell structure of β-Li_2TiO_3, structure of which is referenced from Kataoka et al. [8].

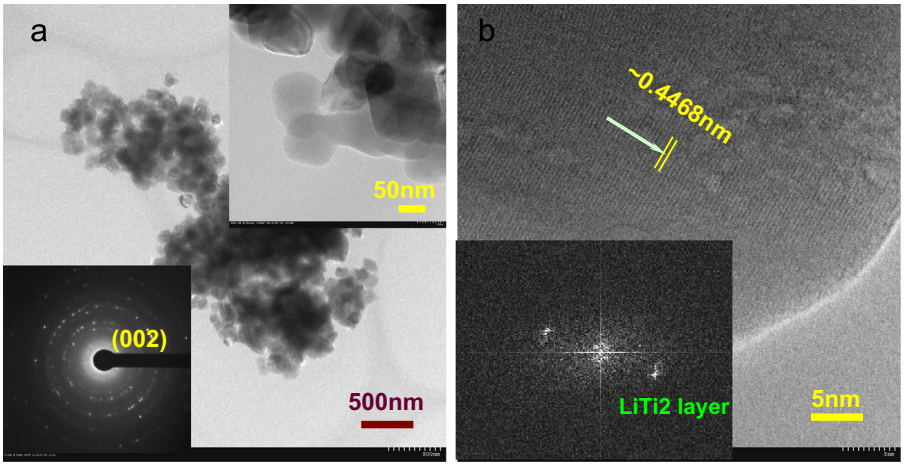

Fig. 7. (a) TEM image, SAED pattern and (b) HR-TEM image, 2DFFT pattern of the Li_2TiO_3 by further calcination at 600 °C.

TEM images and particle size analysis of the particles via hydrothermal reaction and those calcined at 500 °C and 600 °C for 6 h are given in Fig. 4(a–c), correspondingly. From the morphology and the particle size analysis results, the general size for the particles synthesized by hydrothermal reaction is around 114 nm with no obvious increase when calcined at 500 °C and 600 °C.

The morphology of the particles via hydrothermal reaction and that calcined at 500 °C and 600 °C for 6 h are given in Fig. 5(a–c), correspondingly. From the micrograph of the particles via hydrothermal reaction, the mean particle size ranges from 80 nm to 150 nm. There are smaller particles with size of about 50 nm as well. From the micrographs of the particles calcined at 500 °C and 600 °C, no obvious increase of the particle size is exhibited, indicating that no obvious growth takes place during calcination.

3.3. Structure from HR-TEM

TEM image and the SAED pattern of the Li_2TiO_3 via hydrothermal reaction are given in Fig. 6(a). From the SAED pattern, the (002) diffraction ring is not exhibited, indicating the disordering of the atoms in the corresponding lattice plane. HR-TEM image and the corresponding 2DFFT pattern are given in Fig. 6(b). From the HR-TEM image, the layered structure with an average interplanar distance of 0.4805 nm is clearly developed, which corresponds to that of the LiTi2 slab along the *c* axis. The inserted 2DFFT pattern of the HR-TEM confirms the layered structure along the *c* axis. It is interesting that in the interslab of pure Li layer, transferred periodic pattern is exhibited. The structure inferred from this transferred periodic pattern is not perpendicular to LiTi2 slab, thus has to be ascribed to that in the interslab of the pure Li layer. As the white dots in the lattice fringe by HR-TEM are the [TiO6] units, thus the periodic structure in the Li layer contains Ti ions, which possibly results from the residual Ti ions in the Li interslab. In other words, in the interslab of the supercell formed via hydrothermal reaction, there are some residual Ti ions, which is also the possible reason for the collapse of (002) supercell reflection peak. The Li/Ti ratio is 1.48 by ICP-AES, indicating the structure of Li_2TiO_3 via hydrothermal reaction is Li deficient.

It needs to be addressed that the structure of the Li_2TiO_3 via hydrothermal treatment is also reasonable the cubic phase. As claimed recently by Lamman and co-workers [13], a cubic phase Li_2TiO_3 is formed by hydrothermal reaction using TiO_2

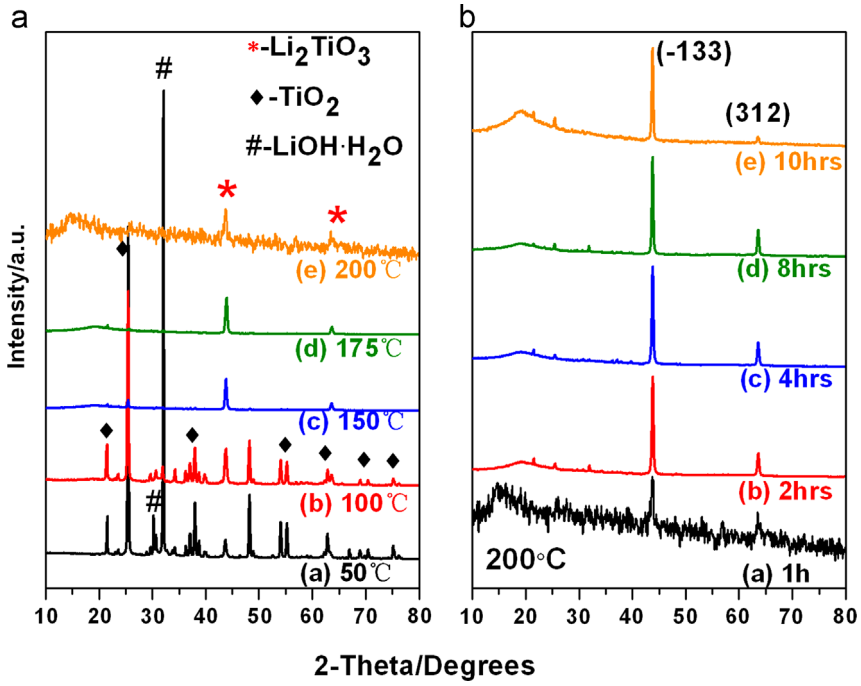

Fig. 8. XRD patterns of the Li_2TiO_3 particles, (a) at varied reaction temperatures and (b) at varied lengths of hydrothermal reaction time.

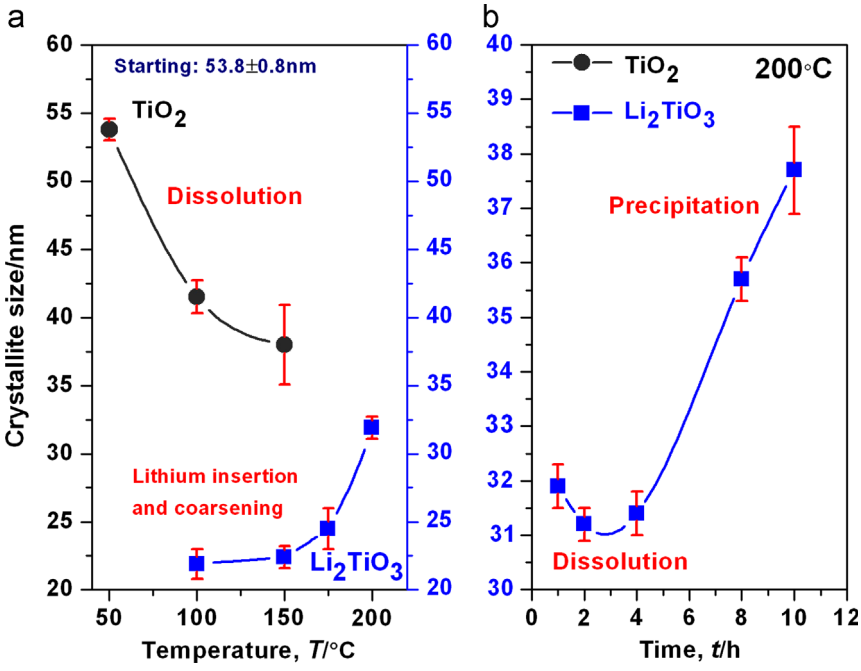

Fig. 9. Crystallite size evolution of the TiO_2 and Li_2TiO_3 particles, (a) at varied reaction temperatures and (b) at varied lengths of hydrothermal reaction time.

and LiOH. By the structure refinement of the patterns of neutron diffraction, a cubic phase with space group Fm-3m is determined, in which the Li ions and Ti ions occupy the 4a wickoff sites. By further calcinations at above 300 °C, transformation from cubic into monoclinic takes place, forming a more stable structure.

TEM image and the SAED pattern of the Li_2TiO_3 calcined at 600 °C in air for 6 h are given in Fig. 7(a). Compared with the SAED pattern in Fig. 6(a), the (002) diffraction ring is exhibited, indicating the ordering of the atoms in the corresponding lattice plane. From the HR-TEM image in Fig. 7(b), the layered structure with an average interplanar distance of 0.4468 nm which corresponds to that of the LiTi2 layer along the *c* axis is clearly developed. The inserted 2DFFT pattern of the HR-TEM confirms the layered structure along the *c* aixs. In contrast, in the interslab of pure Li layer, no transferred periodic pattern is exhibited, indicating that almost no residual Ti ions are in the Li1Li2 layer. Ti ions may have diffused away

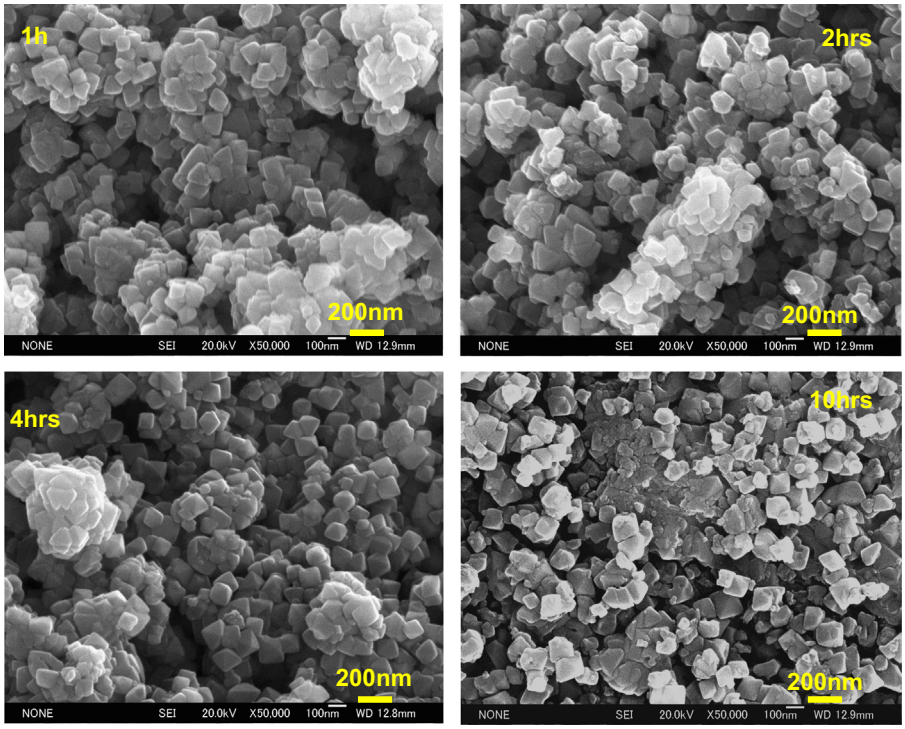

Fig. 10. FE-SEM micrographs of the Li_2TiO_3 particles at 200 °C for varied lengths of time, (a) 1 h; (b)2 h; (c)4 h; and (d)10 h.

from the interslab into the slab, occupying the vacancies or substituting the Li ions, forming the final monoclinic Li_2TiO_3. The Li/Ti ratio is determined as 1.998 by ICP-AES, which confirms that additional Li ions have diffused into the supercell during calcination.

3.4. Formation mechanism of Li_2TiO_3

According to the extensive experimental results, a preferred development of (−133) diffraction peak (for the monoclinic phase) is always exhibited in the XRD patterns of the particles via hydrothermal reaction, indicating a preferred well ordering of the atoms in this lattice plane. For a perfect structure of Li_2TiO_3, in the (−133) lattice plane, two titanium ions together with one lithium ion in the 4e wickoff sites are ordered in the slab. As the starting particles are anatase TiO_2, the insertion of lithium ions into the cell is reasonable during hydrothermal reaction. According to the research by Tielens et al., the preferred site for occupation of lithium during insertion is the empty distorted octahedron centered at 4b special positions [15]. Once the insertion takes place, the basic structure of (−133) lattice plane is formed. However, in this structure unit, abundant lithium ions are introduced and the $[LiO_{6-a}OH_a]$ and $[TiO_{6-b}OH_b]$ $(0 < a,\ b < 6)$ octahedra are not well ordered. According to our previous research, the octahedra can undergo distortion and re-adjustment providing the adding of OH^- during hydrothermal reaction or in water vapor at higher temperature [14].

XRD patterns of the particles in the heating process from room temperature to 200 °C and that held at 200 °C for varied lengths of time are shown in Fig. 8(a) and (b), respectively. It is obvious that when the autoclave is heated to 175 °C, only residual trace TiO_2 is exhibited; and the diffraction peak (−133) of Li_2TiO_3 emerges from 100 °C, indicating the formation of Li_2TiO_3. From Fig. 8(b), pure phase Li_2TiO_3 is formed at 200 °C.

The crystallite size evolution of the raw TiO_2 and the Li_2TiO_3 particles from room temperature to 200 °C and that held at 200 °C for varied lengths of time are shown in Fig. 9(a) and (b), respectively. From Fig. 9(a), the crystallite size of TiO_2 decreases from 53.8 nm at 50 °C to 38 nm at 150 °C, and only trace TiO_2 can be observed at 175 °C, which indicates that most of the TiO_2 has been transformed into Li_2TiO_3, during which the decrease of the TiO_2 crystallite size confirms the dissolution of the raw TiO_2. It is interesting that in pure water, the crystallite size of TiO_2 decreases to 36.9 nm at 200 °C for 10 h, while it decreases to 38 nm at 150 °C for only 1 h in LiOH solution, which confirms the estimation discussed in Section 3.1. On the other hand, an obvious increase of the crystallite size of the Li_2TiO_3 from 21.9 nm at 100 °C to 27.4 nm at 150 °C, and to 32 nm at 200 °C is exhibited, confirming the reasonable insertion of lithium ions into the TiO_2 and the coarsening of Li_2TiO_3 crystallite during hydrothermal reaction.

From Fig. 9(b), during the hydrothermal reaction at 200 °C, a previous decrease of the crystallite size before 4 h and an obvious increase from 4 h to 10 h are clearly exhibited. The ongoing hydrothermal reaction will induce the dissolution and precipitation process of the crystal growth. Two possible processes can take place, one of which is that isolated $[TiO_{6-b}(OH)_b]$ octahedra reconstruct and precipitate on the stable Li_2TiO_3 nuclei, the other of which is that $[TiO_{6-b}(OH)_b]$ octahedra clusters undergo adjustment and precipitate on the

Li_2TiO_3 nuclei stably formed. The latter is preferred and is the so-called in-situ crystallization or solid state epitaxial crystallization [16–18].

Fig. 10 shows the FE-SEM micrographs of the Li_2TiO_3 particles at 200 °C for 1 h, 2 h, 4 h, and 10 h. Small particles with diameters less than 40 nm are formed when reacted for 4 h compared with that for 2 h. With time increasing, these small particles grow larger, which can be served as another evidence for the formation mechanism of Li_2TiO_3 to be dissolution and precipitation.

4. Conclusions

Li_2TiO_3 nano-particles were synthesized via hydrothermal reaction using microsized anatase TiO_2 and LiOH with stoichiometric Li/Ti ratio and LiOH concentration of 2 mol/L. 5 Conclusions are drawn as follows:

(1) The crystallite size of TiO_2 obviously decreases from 53.8 nm to 36.9 nm after hydrothermal treatment in distilled water, indicating that the dissolution takes place.
(2) No development of the (002) supercell diffraction peaks in the XRD pattern is exhibited by hydrothermal reaction. In contrast, full development is exhibited by calcination above 500 °C for 6 h in air.
(3) The general particle size is about 114 nm, and no obvious increase in particle size is observed during further calcinations.
(4) HR-TEM analysis shows that the layered structure corresponding to that of the LiTi2 layer along the *c* axis is clearly developed. After calcination, the ordering of the atoms in the lattice plane is confirmed by the exhibition of (002) diffraction ring in the SAED pattern and additional Li ions diffuse into the supercell, corresponding with the diffusion of Ti ions away from the interslab into the slab.
(5) Lithium ions insertion into TiO_2 corresponding with the dissolution of TiO_2 takes place during the hydrothermal reaction and for the formation of Li_2TiO_3, the $[LiO_{6-a}OH_a]$ and $[TiO_{6-b}OH_b]$ $(0 < a,\ b < 6)$ octahedra adjust with ongoing dissolution and precipitation for the crystal growth.

Acknowledgments

The authors are grateful to Prof. Larry G. Olson from Chang'an University, PR China for improving the English presentation.

References

[1] T. Hoshino, M. Nakamichi, Development of fabrication technologies for advanced breeding functional materials for DEMO reactors, Fusion Engineering and Design 87 (2012) 486–492.
[2] K. Kondo, Y. Tatebe, K. Ochiai, S. Sato, K. Takakura, S. Ohnishi, C. Konno, Measurement of TPR distribution in natural Li_2TiO_3/Be assembly with DT neutrons, Fusion Engineering and Design 85 (2010) 1229–1233.
[3] R. Ramaraghavulu, S. Buddhudu, G. Bhaskar Kumar, Analysis of structural and thermal properties of Li_2TiO_3 ceramic powders, Ceramics International 37 (2011) 1245–1249.
[4] I. Tazhibayeva, I. Beckman, V. Shestakov, A. Kiykabaeva, H. Kawamura, K. Tsuchiya, Tritium accumulation and release from Li_2TiO_3 during long-term irradiation in the WWR-K reactor, Journal of Nuclear Materials 417 (2011) 748–752.
[5] M. Castellanos, A.R. West, Order-disorder phenomena in oxides with rock salt structures: the system Li_2TiO_3–MgO, Journal of Materials Science 14 (1979) 450–454.
[6] M.D. Aguas, G.C. Coombe, I.P. Parkin, New solid state routes to lithium transition metal oxides via reactions with lithium oxide, Polyhedron 17 (1998) 49–53.
[7] G. Bhaskar Kumar, S. Buddhudu, Synthesis and emission analysis of RE^{3+} (Eu^{3+} or Dy^{3+}): Li_2TiO_3 ceramics, Ceramics International 35 (2009) 521–525.
[8] K. Kataoka, Y. Takahashi, N. Kijima, H. Nagai, J. Akimoto, Y. Idemoto, K. Ohshima, Crystal growth and structure refinement of monoclinic Li_2TiO_3, Materials Research Bulletin 44 (2009) 168–172.
[9] X. Wu, Z. Wen, B. Lin, X. Xu, Sol–gel synthesis and sintering of nano-size Li_2TiO_3 powder, Materials Letters 62 (6–7) (2008) 837–839.
[10] C.H. Jung, J.Y. Park, S.J. Oh, H.K. Park, Y.S. Kim, D.K. Kim, J.H. Kim, Synthesis of Li_2TiO_3 ceramic breeder powders by the combustion process, Journal of Nuclear Materials 253 (1998) 203–212.
[11] A. Sinha, S.R. Nair, P.K. Sinha, Single step synthesis of Li_2TiO_3 powder, Journal of Nuclear Materials 399 (2010) 162–166.
[12] C.H. Jung, S.J. Lee, W.M. Kriven, J.Y. Park, W.S. Ryu, A polymer solution technique for the synthesis of nano-sized Li_2TiO_3 ceramic breeder powders, Journal of Nuclear Materials 373 (2008) 194–198.
[13] A. Laumann, K.T. Fehr, M. Wachsmann, M. Holzapfel, B.B. Iversen, Metastable formation of low temperature cubic Li_2TiO_3 under hydrothermal conditions-its stability and structural properties, Solid State Ionics 181 (2010) 1525–1529.
[14] T. Kozawa, A. Onda, K. Yanagisawa, Accelerated formation of barium titanate by solid-state reaction in water vapor atmosphere, Journal of the European Ceramic Society 29 (2009) (3259–3246).
[15] F. Tielens, M. Calatayud, A. Beltrán, C. Minot, J. Andrés, Lithium insertiaon and mobility in the TiO_2-anatase/titanate structure: a periodic DFT study, Journal of Electroanalytical Chemistry 581 (2005) 216–223.
[16] J. Ovenstone, K. Yanagisawa, Effect of hydrothermal treatment of amorphous titania on the phase change from anatase to rutile during calcinations, Chemistry of Materials 11 (10) (1999) 2770–2774.
[17] K. Yanagisawa, J. Ovenstone, Crystallization of anatase from amorphous titania using the hydrothermal technique: effects of starting material and temperature, Journal of Physical Chemistry B 103 (37) (1999) 7781–7787.
[18] K. Yanagisawa, Y. Yamamoto, Q. Feng, N. Yamassaki, Formation mechanism of fine anatase crystals from amorphous titania under hydrothermal conditions, Journal of Materials Research 13 (4) (1998) 825–829.